A structurally precise mechanism links an epilepsy-associated *KCNC2* potassium channel mutation to interneuron dysfunction

Jerome Clatot[a,b,1], Christopher B. Currin[c,1], Qiansheng Liang[d] (ID), Tanadet Pipatpolkai[e], Shavonne L. Massey[a,b,f], Ingo Helbig[a,b,f,g], Lucie Delemotte[e] (ID), Tim P. Vogels[c] (ID), Manuel Covarrubias[d,2], and Ethan M. Goldberg[a,b,f,h,2] (ID)

De novo heterozygous variants in *KCNC2* encoding the voltage-gated potassium (K⁺) channel subunit Kv3.2 are a recently described cause of developmental and epileptic encephalopathy (DEE). A de novo variant in *KCNC2* c.374G > A (p.Cys125Tyr) was identified via exome sequencing in a patient with DEE. Relative to wild-type Kv3.2, Kv3.2-p.Cys125Tyr induces K⁺ currents exhibiting a large hyperpolarizing shift in the voltage dependence of activation, accelerated activation, and delayed deactivation consistent with a relative stabilization of the open conformation, along with increased current density. Leveraging the cryogenic electron microscopy (cryo-EM) structure of Kv3.1, molecular dynamic simulations suggest that a strong π-π stacking interaction between the variant Tyr125 and Tyr156 in the α-6 helix of the T1 domain promotes a relative stabilization of the open conformation of the channel, which underlies the observed gain of function. A multicompartment computational model of a Kv3-expressing parvalbumin-positive cerebral cortex fast-spiking γ-aminobutyric acidergic (GABAergic) interneuron (PV-IN) demonstrates how the Kv3.2-Cys125Tyr variant impairs neuronal excitability and dysregulates inhibition in cerebral cortex circuits to explain the resulting epilepsy.

epilepsy | neurogenetics | KCNC2 | Kv3.2 | potassium channels

Potassium (K⁺) channels set the resting membrane potential of neurons, mediate repolarization of the action potential, and regulate neurotransmitter release and synaptic plasticity, among other functions, and hence are critical determinants of neuronal excitability (1). K⁺ channels are the most diverse of the ion channel superfamily, being organized into families and subfamilies based on DNA sequence similarities. Among these, the voltage-gated K⁺ (Kv) channels constitute the largest subfamily (2).

Given the biological importance and variety of voltage-gated K⁺ channels, it is not surprising that pathogenic variants in many K⁺ channel genes have been identified as causes of neurological disease including epilepsy. Of the more than 70 known K+ channel genes, 15 have been linked to epilepsy, with the main mechanism being de novo variation. In fact, the K⁺ channel subunit gene *KCNQ2* is the second most commonly identified gene in epilepsy (3). Such K⁺ channels represent potential targets for development of directed pharmacotherapy. Members of the Kv3 subfamily contribute to high-frequency firing of defined subsets of neurons throughout the nervous system, based on a coordinated and unique set of biophysical properties, including a depolarized voltage dependence of activation and rapid activation and deactivation kinetics (4, 5). Parvalbumin-positive fast-spiking GABAergic interneurons (PV-INs) specifically express Kv3.1 and Kv3.2 which determines the fast-spiking phenotype of these cells (6–9); recent work using cell type–specific proteomics in mice confirmed that *Kcnc2* is among the most highly differentially expressed proteins in neocortical PV-INs (10). Variants in the Kv3 subfamily member gene *KCNC1* cause a spectrum of neurologic disorders including developmental delay/intellectual disability, progressive myoclonus epilepsy, and early-onset developmental and epileptic encephalopathy (DEE) (11–15). Mice lacking Kv3.2 exhibit abnormal EEG patterns and increased susceptibility to PTZ-induced seizures, supporting the role of *KCNC2* in human disease (7). De novo variants in *KCNC2* were only recently identified as a novel cause of epileptic encephalopathy; however, the pathophysiological mechanisms remain poorly understood (16–22).

Here, we describe a patient with DEE found to harbor a de novo variant in *KCNC2*, c.374G > A (p.Cys125Tyr). This variant produces a missense substitution p.Cys125Tyr located near the α-6 helix of the cytoplasmic tetramerization domain (cT1D) of the Kv3.2 channel subunit (*SI Appendix*, Fig. S1). In addition to determining specific subunit tetramerization between members of the same Kv channel subfamily, the cT1D plays multiple roles in Kv channel function, serving as a docking site for cytoplasmic accessory subunits, regulating subcellular targeting, and controlling channel gating (23–25).

Significance

A novel variant in *KCNC2*—a gene encoding the potassium channel subunit Kv3.2—was identified in a patient with childhood-onset epilepsy and developmental disability. The variant channel exhibits electrophysiological abnormalities consistent with gain of ion channel function driven by a structural change in the cytoplasmic T1 domain known to be involved in tetramerization of Kv channels yet with emerging roles in regulation of channel gating. However, a computational model demonstrates loss of function with impaired excitability of a Kv3.2-expressing fast-spiking parvalbumin-positive GABAergic inhibitory interneuron, which may lead to disinhibition and instability of cerebral cortex circuits underlying epilepsy.

The role of the cT1D in gating involves noncanonical interactions primarily governed by the α-6 helix of the cT1D, as demonstrated by the recently reported cryo-EM structure of Kv3.1a, which revealed substantial differences in the conformation of the cT1D when compared to that of Kv1.2 channels despite an overall similar architecture (26). This cryo-EM study unexpectedly revealed that the α-6 helix of the cT1D in Kv3 and Kv4 channels is in close proximity to regions canonically involved in channel gating (e.g., the S4 to S5 linker and S6) (26, 27). As the Cys125Tyr variant is in the cT1D of Kv3.2, we hypothesize here that the gain of function (GoF) effect of p.Cys125Tyr with a large hyperpolarizing shift in the voltage dependence of activation results from disruption of these critical interactions. We seek to use the recently determined cryo-EM structure of Kv3 channels to investigate the mechanism whereby *KCNC2* c.374G>A (p.Cys125Tyr) leads to neurological disease. Electrophysiological, mutagenesis, and biophysical analyses combined with molecular dynamics (MDs) simulations strongly suggest that a novel π-π stacking interaction in the cT1D underlies the mechanism whereby p.Cys125Tyr induces a prominent effect on gating with a large hyperpolarizing shift in the voltage dependence of activation representing a gain of channel function. Furthermore, we employed computational modeling to elucidate a precise mechanism whereby gain of Kv3.2 channel function leads to impaired excitability of Kv3.2-expressing fast-spiking GABAergic interneurons.

Results

Identification of a Novel *KCNC2* Variant Associated with Epileptic Encephalopathy. We identified a de novo variant *KCNC2* c.374G>A (p.Cys125Tyr) (*SI Appendix*, Fig. S1) in a then 6-y-old girl with treatment-resistant mixed epilepsy (generalized and focal epileptiform activity), hypotonia, speech delay/arrest/regression, and autism spectrum disorder. The patient was a female born to nonconsanguineous parents at term without pre- or perinatal complications. The clinical course was unremarkable until 3 mo of age when the patient experienced a first unprovoked seizure, described as clonic jerking of the bilateral upper and lower extremities and face. Continuous video electroencephalography at age 7 mo demonstrated a high-voltage, disorganized background in sleep with multifocal epileptiform discharges in the central midline, right central, frontal, and anterior temporal regions, and six electroclinical seizures over the course of approximately 72 h characterized by diffuse onset of rhythmic delta slowing with evolution of focal slowing and/or spike-wave discharges in the bicentral or bilateral frontal regions accompanied by rhythmic clonic activity of the bilateral face and extremities. MRI of the brain at age 8 mo was unremarkable. No dysmorphic features were noted. Trials of the antiseizure medications oxcarbazepine, prednisolone, and topiramate were with limited response. By age 2 y, there was regression of previously acquired language, and the patient was noted to be nonverbal. Lamotrigine therapy was initiated, and seizure frequency decreased significantly; the patient remained seizure-free on lamotrigine monotherapy for 2 y, and repeat EEGs performed during this time were normal in wakefulness and sleep. Then, at age 5 y, the patient presented with altered mental status characterized by urinary incontinence and decreased responsiveness; EEG revealed generalized spike-wave stupor characterized by persistent 1 to 2 Hz generalized spike-and-wave discharges. The patient continued to cycle in and out of this electroclinical pattern for the ensuing year despite treatment with various antiseizure medications (clobazam, felbamate, lamotrigine, levetiracetam, and valproic acid). Developmental history was notable for language regression at 2 y,

and the patient remained nonverbal at the most recent follow-up; she was diagnosed with autism spectrum disorder at age 3 y. At age 6 y, neurologic examination showed truncal and appendicular hypotonia; there was no ataxia. At the last visit at age 7 y, the patient remained nonverbal; epilepsy continued to be treated with felbamate and clobazam. Repeat EEG showed a slow, underdeveloped waking background, with intermittent independent slowing of the bilateral temporal and/or bilateral frontal regions, bifrontal predominant irregularly generalized sharp-wave discharges, bifrontal sharp wave discharges, and subclinical seizures with bifrontal onset.

Trio whole exome sequencing identified a de novo heterozygous pathogenic variant in *KCNC2* c.374G > A (p.Cys125Tyr) which is not present in the Exome Aggregation Consortium or genome Aggregation Database (http://gnomad.broadinstitute.org) and has a corresponding CADD score of 24.9 (28). The identified variant was interpreted according to the American College of Medical Genetics and Genomics standards and guidelines for the interpretation of sequence variants. This variant is localized to the intracellular N terminus of the protein and converts the small sulfur-containing cysteine residue to a larger, polar tyrosine residue containing an aromatic side chain, which is associated with a Grantham's distance of 194 (indicating greater evolutionary distance and a higher likelihood that the substitution is damaging to protein structure/function) (29). The patient did not carry any other variants classified as pathogenic or likely pathogenic and no other de novo variants were identified in other ion channel or epilepsy-associated genes. Prior work identified a heterozygous de novo pathogenic variant *KCNC2* c.375C > G (p.Cys125Trp) located at the same amino acid residue in a child with a similar phenotype of mild-to-moderately severe global developmental delay, hypotonia, autism spectrum disorder, and treatment-resistant epilepsy with multiple seizure types (22), further supporting the pathogenic nature of the identified variant.

We expressed wild type (WT) or variant *KCNC2* cDNA in HEK-293T cells for whole-cell voltage-clamp recording of ionic currents, as well as a combination of WT + variant (in a 1:1 equimolar ratio) to mimic the heterozygous state of the variant in the patient. We then performed whole-cell voltage-clamp recording of ionic currents. These conditions all yielded a rapidly activating outward current with little/no inactivation (Fig. 1 *A–C*). We found that cells expressing *KCNC2*-p.Cys125Tyr alone or in combination with WT exhibited a larger peak outward current than cells expressing WT alone. At 0 mV, peak current density was 106.2 ± 40.2 pA/pF for WT (n = 12 cells), 689.2 ± 93.5 pA/pF for variant (n = 22 cells; $P < 0.001$ vs. WT via one-way ANOVA), and 497.6 ± 59.7 pA/pF for WT + variant (n = 28; $P < 0.001$ vs. WT via one-way ANOVA) (Fig. 1 *A–D* and Table 1). In addition, we observed a marked –32.7 mV leftward (hyperpolarized) shift in the voltage dependence of channel activation: The $V_{1/2}$ of activation was 7.9 ± 1.5 mV for WT alone (n = 12), –24.8 ± 1.1 mV for variant *KCNC2*-p.Cys125Tyr (n = 22; $P < 0.001$ vs. WT), and –7.3 ± 2.4 mV for WT + variant (n = 28) (Fig. 1*E* and Table 1). Expression of the *KCNC2*-p.Cys125Tyr variant alone hyperpolarized transfected cells to –64.9 ± 2.2 mV while WT + variant hyperpolarized cells to –62.2 ± 2.0 mV, relative to a resting membrane potential of –32.8 ± 1.7 mV for WT ($P < 0.001$ vs. WT; Table 1). We also observed an acceleration in the kinetics of activation and slowing of deactivation in the *KCNC2*-p.Cys125Tyr variant relative to WT (Figs. 1*F* and 2*D* and Table 1). When expressed with WT, the *KCNC2*-p.Cys125Tyr variant accelerated the kinetics of activation beyond that produced by the variant alone, while coexpression of WT and variant led to a deactivation kinetics that was intermediate between WT and variant alone (Fig. 2 and Table 1).
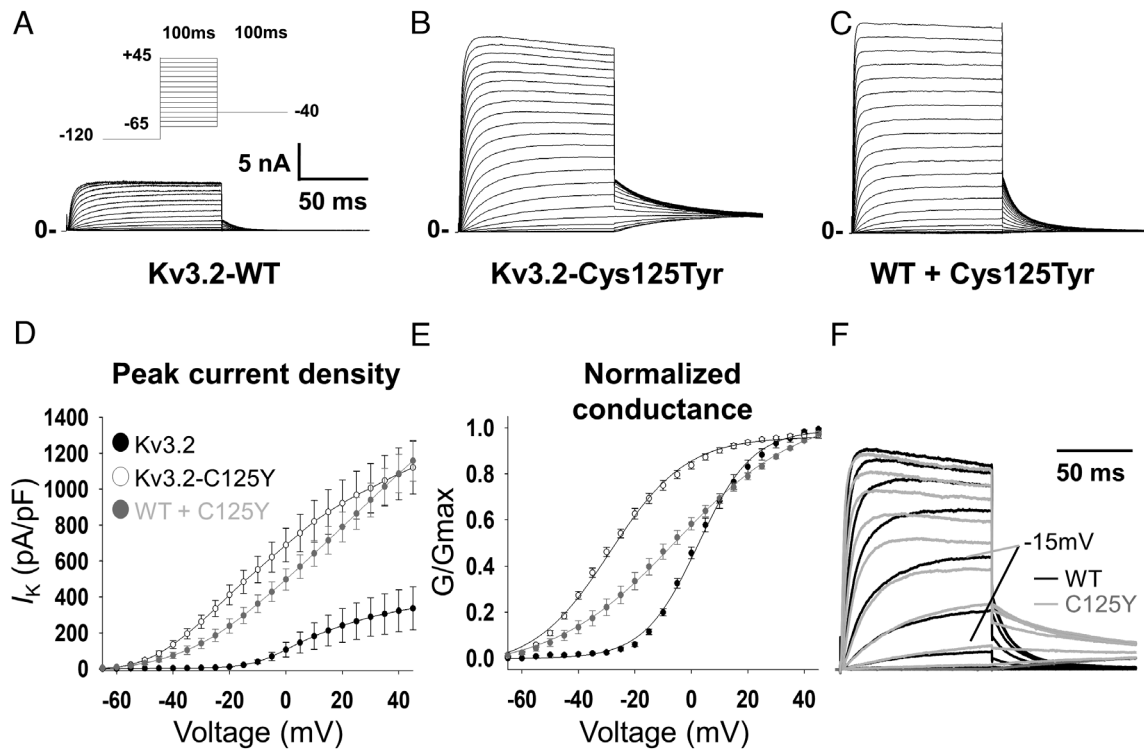
Fig. 1. Electrophysiological properties of Kv3.2 and the epilepsy-associated Kv3.2-Cys125Tyr variant in a heterologous system. (*A*) Representative trace for wild-type Kv3.2 (Kv3.2-WT), which gives rise to a delayed rectifier type K+ current in a heterologous cell system. The epilepsy-associated variant Kv3.2-Cys125Tyr (*B*) and coexpressed WT + Kv3.2-Cys125Tyr variant exhibit a dramatic increase in peak current density (*C*). (*D*) Plot of current density (in pA/pF) vs. voltage illustrates the left shift in voltage dependence of activation and increased current density of Kv3.2-Cys125Tyr and WT + Kv3.2-Cys125Tyr relative to WT alone. (*E*) Leftward (hyperpolarized) shift in the conductance-voltage (*G/G*$_{max}$) curve for Kv3.2-Cys125Tyr compared to WT. (*F*) Superimposed representative traces for WT and Kv3.2-Cys125Tyr variant illustrate accelerated activation kinetics for the Cys125Tyr variant relative to WT, with the response to a voltage step to −15 mV highlighted for clarity. Closed circles/bars indicate Kv3.2-WT; open circles/bars indicate Kv3.2-Cys125Tyr; gray circles/bars indicate Kv3.2-WT + Kv3.2-Cys125Tyr. *n* = 12 to 28 cells per genotype from *N* = 4 or more separate transfections. ***P < 0.001 via one-way ANOVA.

The combination of increased current density and hyperpolarized voltage dependence of activation along with accelerated kinetics of activation and slowed kinetics of deactivation suggest a GoF effect of the p.Cys125Tyr variant. The voltage- and time-dependent changes underlying the GoF phenotype suggest a robust relative stabilization of the open state of the channel. Further validation of this striking finding was obtained upon expression in *Xenopus laevis* oocytes, which revealed the same effects of *KCNC2*-p.Cys125Tyr under two-electrode voltage-clamp (TEVC) conditions (Fig. 3 *A–D* and *SI Appendix,* Table S1).

The recent cryo-EM structure of Kv3.1 demonstrated a novel role for the cT1D in the control of channel gating (26). To determine whether the paralogous variant in Kv3.1 might exert a similar effect on gating, we tested Kv3.1-Cys78Tyr in *Xenopus* oocytes under TEVC conditions and found a marked left-shift in the voltage dependence of activation (Fig. 3 *E–H* and

SI Appendix, Table S2), while accelerating activation and slowing deactivation (Fig. 3*H*). To further elucidate the significance of the Cys78 residue, we mutated this amino acid to alanine and observed a left-shift in the voltage dependence of activation and altered gating kinetics (Fig. 3 *F* and *G*), although this was not as dramatic as that seen for Kv3.1-Cys78Tyr. In HEK-293T cells, Kv3.2-Cys125Ala also produced a small left-shift in the voltage dependence of activation, with a corresponding acceleration of activation and slowing of deactivation (*SI Appendix,* Fig. S2).

Structural Changes Involving the α-6 Helix of the cT1D Underlie the GoF Phenotype of Kv3.1-Cys78Tyr and Kv3.2-Cys125Tyr. To elucidate the structural basis of the GoF phenotype of the currents induced by the Kv3.1-Cys78Tyr, Kv3.1-Cys78Ala, and Kv3.2-Cys125Tyr, we utilized the published cryo-EM structure of Kv3.1

Table 1. Biophysical properties of WT and variant hKv3.2-p.Cys125Tyr in HEK-293 cells

Group	Peak current density (at 0 mV)	Voltage dependence of activation (*V*$_{1/2}$)	Time constant of activation (at +10 mV)	Time constant of deactivation (at −70 mV)	Resting membrane potential *V*$_m$	*n*
	pA/pF	mV	t (ms)	t (ms)	*V*$_{1/2}$	
Kv3.2-WT	106.2 ± 40.2	7.9 ± 1.5	12.0 ± 1.9	2.5 ± 0.1	−32.8 ± 1.7	12
Cys125Tyr	689.2 ± 93.5***	−24.8 ± 1.1***	2.7 ± 0.5*	10.8 ± 0.5***	−64.9 ± 2.2	22
WT + Cys125Tyr	497.6 ± 59.7***	−7.3 ± 2.4***	1.5 ± 0.2***	5.1 ± 0.7**	−62.2 ± 2.0	28

*P < 0.05;
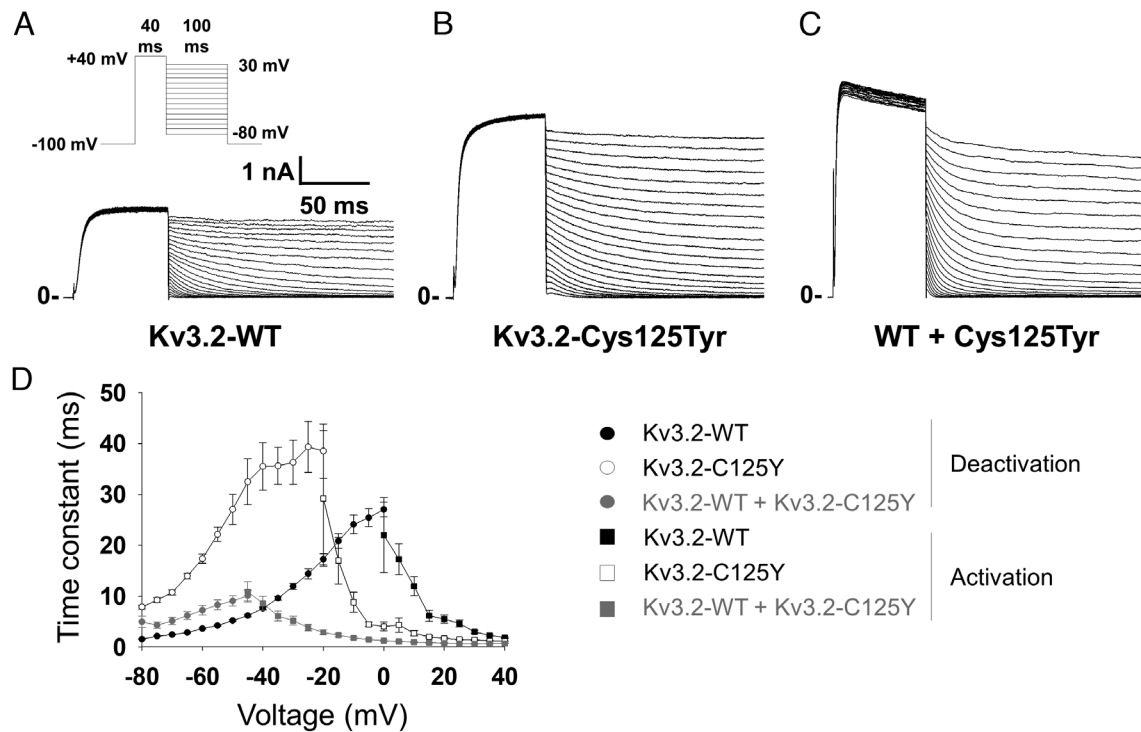**P < 0.01; and
***P < 0.001; vs. WT via one-way ANOVA.

Fig. 2. Altered gating kinetics associated with the *KCNC2*-p.Cys125Tyr variant. (*A*) Example trace with protocol (*Inset*) illustrating the recording of the kinetics of deactivation for WT Kv3.2. (*B*) Deactivation of Kv3.2-Cys125Tyr. (*C*) Deactivation of WT + variant Kv3.2-Cys125Tyr. (*D*) Summary data showing accelerated activation (from the data in Fig. 1) and slowed deactivation for Kv3.2-Cys125Tyr and WT + Kv3.2-Cys125Tyr relative to WT alone. Circles indicate deactivation, while squares indicate activation; closed symbols indicate WT, open symbols indicate Kv3.2-Cys125Tyr, and gray symbols indicate WT + Kv3.2-Cys125Tyr. Data are from *n* = 12 to 28 cells per genotype from *N* = 4 or more separate transfections.

and conducted 2 repeats of 700 ns MD simulations per Kv3.1 and Kv3.2 construct (26), allowing a total of eight datasets to be curated per each condition (*Materials and Methods*). Previous structural and electrophysiological studies suggest that interactions involving the α-6 helix of the T1 domain regulate Kv3.1 voltage dependence of activation (26). Thus, we hypothesized that changes in the α-6 helix conformation and flexibility induced by the substitutions described here may underlie the biophysical GoF phenotype. To test this hypothesis, we identified the residues involved in contact frequency changes near the α-6 helix, which would have resulted from the Cys78Tyr and Cys125Tyr in Kv3.1 and Kv3.2, respectively (Fig. 4*A*). We define the contact frequency as the fraction of simulation frames collected every 20 ps in which any atoms of these two amino acids are within 3 Å from each other for VdW interaction or hydrogen bonding and within 4 Å from each other if the pair is a putative salt bridge (30). Relative to WT, the MD simulations demonstrate that both Kv3.1-Cys78Tyr and Kv3.2-Cys125Tyr mutations greatly increase interaction with Tyr109 and Tyr156 in the α-6 helix, respectively (*P* < 0.001) (Fig. 4 *B* and *C*).

We then calculated the flexibility of the Kv3.1 α-6 helix backbone (residues 110 to 120) by counting the fraction of frames with an rmsd of the C-α atoms >3 Å, indicating a destabilization of the α-6 helix. We used Asp114Ala in the α-6 helix as a positive control, as a previous study showed that Asp114Ala also induces a hyperpolarizing shift in the voltage dependence of channel gating (26). We found that the α-6 helix of the T1 domain exhibits similar differences in C-α atoms (and hence the backbone) flexibility when comparing WT to Cys78Tyr and Asp114Ala. Considering that—like Cys78Tyr—Asp114Ala also induces a relative stabilization of the open conformation of the channel (26), Asp114Ala acts most

significantly to lower α-6 helix flexibility (Fig. 4*D*). Cys78Ala, in contrast, does not change its contact frequency with Tyr109 and α-6 helix flexibility (Fig. 4*B*). Also, Asp114Ala does not impact the contact frequency between Cys78 and Tyr109 (Fig. 4*B*).

To elucidate the structural link between the flexibility of the α-6 helix and the stability of the open state, we additionally measured the contact frequency between Asp114 and Lys451 in the distal segment of S6 that is near the bundle crossing that constitutes the activation gate of the channel. Although Cys78Tyr does not significantly change contact frequency, Cys78Ala and Asp114Ala decrease the contact frequency between Asp114 and Lys451, a potentially important change, as Asp114 and Lys451 may interact via a salt bridge in the closed state (*SI Appendix,* Fig. S4). Thus, a perturbation at Lys451 may mirror the biophysical phenotypes of Asp114Ala. To test this hypothesis, we created Lys451Ala and compared its voltage-dependent activation curve against of Asp114Ala. Consistent with the hypothesis, we found that Lys451Ala and Asp114Ala similarly hyperpolarize the voltage dependence of activation (*SI Appendix,* Fig. S3 and Tables S3 and S4). Moreover, the variant with the double mutation (Lys451Ala + Asp114Ala; 2 Ala) exhibited no evidence of additivity, which is consistent with perturbation of a direct interaction between Asp114 and Lys451 (*SI Appendix,* Fig. S3 and Tables S3 and S4). Perturbation of this interaction, however, may not underlie the relative stabilization of open conformation induced by Cys78Tyr, since this substitution did not decrease the frequency of contact between Asp114 and Lys451 (*SI Appendix,* Fig. S4).

Considering that Kv3.1-Cys78Tyr and Kv3.2-Cys125Tyr induce similar effects on activation gating, combined with the results from the analysis of Kv3.1-Lys451Ala and Kv3.1-Asp114Ala (above), we next tested the equivalent substitutions in Kv3.2
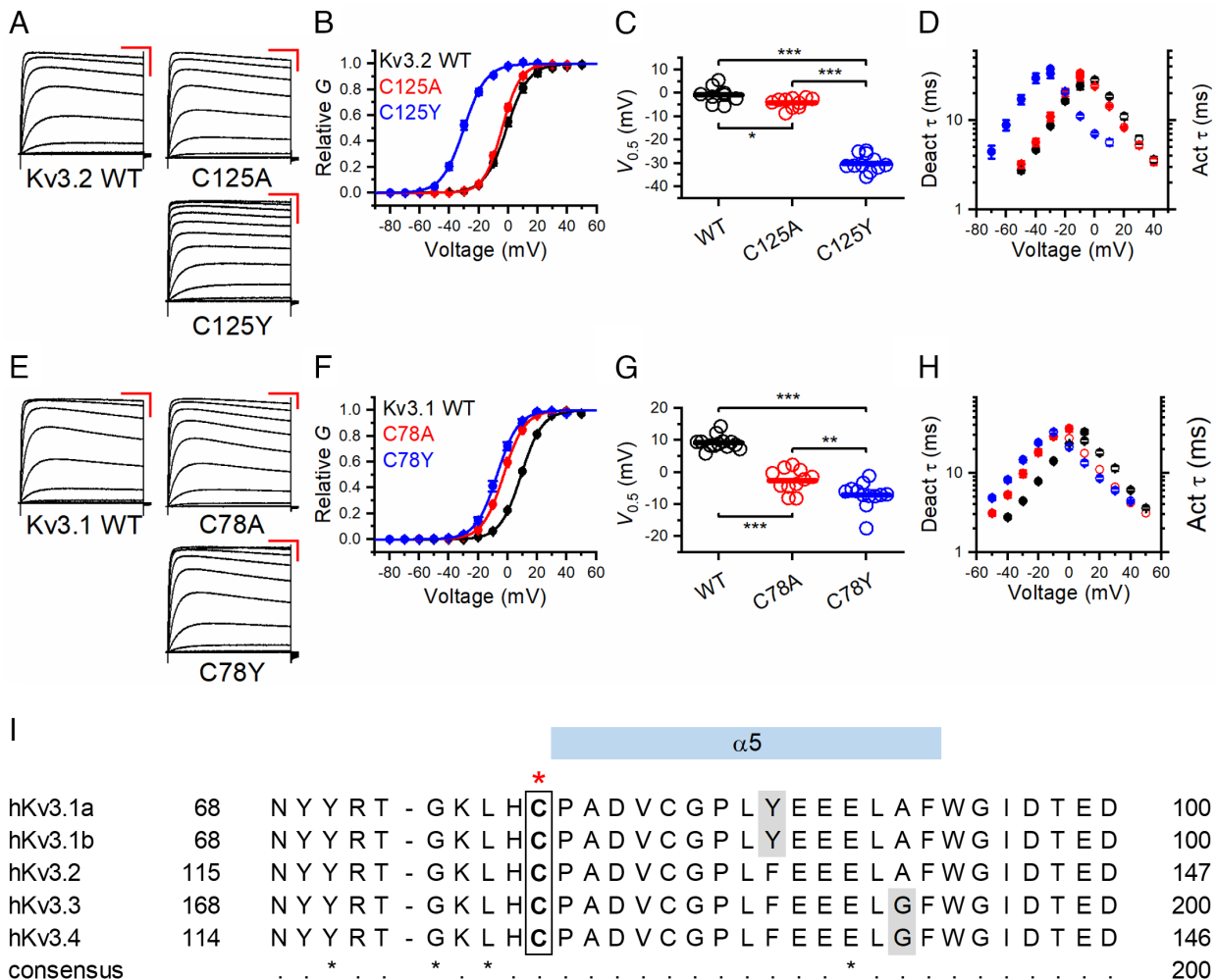
Fig. 3. Voltage-dependent gating and kinetics of Kv3.2 variants C125A and C125Y and Kv3.1 variants Cys78Ala and Cys78Tyr. (*A*) Families of whole-oocyte currents of Kv3.2 WT, Cys125Ala (C125A), and Cys125Tyr (C125Y). Currents were evoked by step depolarizations from a holding voltage of −100 mV. The steps were delivered at 10-s intervals in increments of 10 mV. The scale bars are 100 ms and 1 μA, respectively. (*B*) Normalized peak *G-V* relations of the indicated Kv3.2 variants. The solid lines represent best-fit first-order Boltzmann functions. (*C*) Scatter plots of the midpoint voltage ($V_{1/2}$) determined from the peak *G-V* relations for the indicated Kv3.2 variants. The horizontal line indicates the mean value. (*D*) Voltage dependence of the time constants of deactivation (filled symbols) and activation (hollow symbols) for the indicated Kv3.2 variants. (*E*) Families of whole-oocyte currents of Kv3.1 WT, Cys78Ala, and Cys78Tyr. The protocol and scale bars are as indicated in *A*. (*F*) Normalized peak *G-V* relations of the indicated Kv3.1 variants. The solid lines through the symbols represent best-fit first-order Boltzmann functions. (*G*) Scatter plots of the midpoint voltage ($V_{1/2}$) determined from the peak *G-V* relations for the indicated Kv3.1 variants. The horizontal line indicates the mean value. (*H*) Voltage dependence of the time constants of deactivation (filled symbols) and activation (hollow symbols) for the indicated Kv3.1 variants. (*I*) Sequence alignment of human Kv3 family members around the indicated cysteine residue (in the box and highlighted above by the red star). All amino acids are invariant except those indicated by gray shading (which have high sequence conservation). *$P < 0.05$, **$P < 0.01$, and ***$P < 0.001$ via one-way ANOVA.

(Lys488Ala and Asp161Ala). Relative to WT, Kv3.2-Lys488Ala expressed in either HEK-293T cells or *Xenopus* oocytes exhibited little to no effect on the voltage dependence of the conductance (*SI Appendix*, Figs. S3 and S5). This discrepancy was surprising because Kv3.1 and Kv3.2 are highly conserved in the regions of interest, and MD simulations of Kv3.1 and Kv3.2 suggest that Cys78 and Cys125 are involved in similar interactions (above). However, just like Asp114Ala in Kv3.1, the homologous Asp161Ala in Kv3.2 also induced a significant hyperpolarizing shift that mirrors the effect of Cys125Tyr, a result that is consistent with the role of the α-6 helix in gating control (*SI Appendix*, Fig. S3).

To further probe the structural basis of the discrepancies, we again counted the fraction of frames with rmsd of the C-α atoms of >3 Å to assess the flexibility of the α-6 helix in Kv3.2. In contrast with the results from the Kv3.1 channel, Cys125Tyr destabilizes the α-6 helix, whereas the Lys488Ala shows almost no difference compared to the WT (Fig. 4*E*). We then traced every

possible salt-bridge pair between the α-6 helix (Kv3.1-Asp114, -Glu116, and -Glu117, and Kv3.2-Asp161, -Glu163, and -Glu164) and the S4-S5 linker (Kv3.1-Arg339 and Kv3.2-Arg376), and the S6-helix (Kv3.1-Lys449 and -Lys451, and Kv3.2-Lys486 and -Lys488). This analysis showed that Cys78Ala, Cys78Tyr, and Asp114Ala mutations significantly strengthen the salt bridge between Glu117-Arg339 and weaken the salt bridge between Glu117-Lys449 in Kv3.1 compared to WT (*SI Appendix*, Fig. S4). Also, Cys125Tyr in Kv3.2, decreased contact frequency between Asp161 and Lys488, albeit other potential interactions were not prominent in the Kv3.2 model (*SI Appendix*, Fig. S4). Therefore, a change in the flexibility of the α-6 helix backbone alone may not be the defining factor responsible for the GoF induced by Kv3.1-Cys78Tyr and Kv3.2-Cys125Tyr. Nevertheless, a differential reorganization of a network of salt bridges involved in gating relevant interacions appears to play a role in how perturbations at Cys78 and Cy125 induced a similar GoF phenotype. Moreover, the robust increased interactions of Tyr78 with Tyr109 (in the
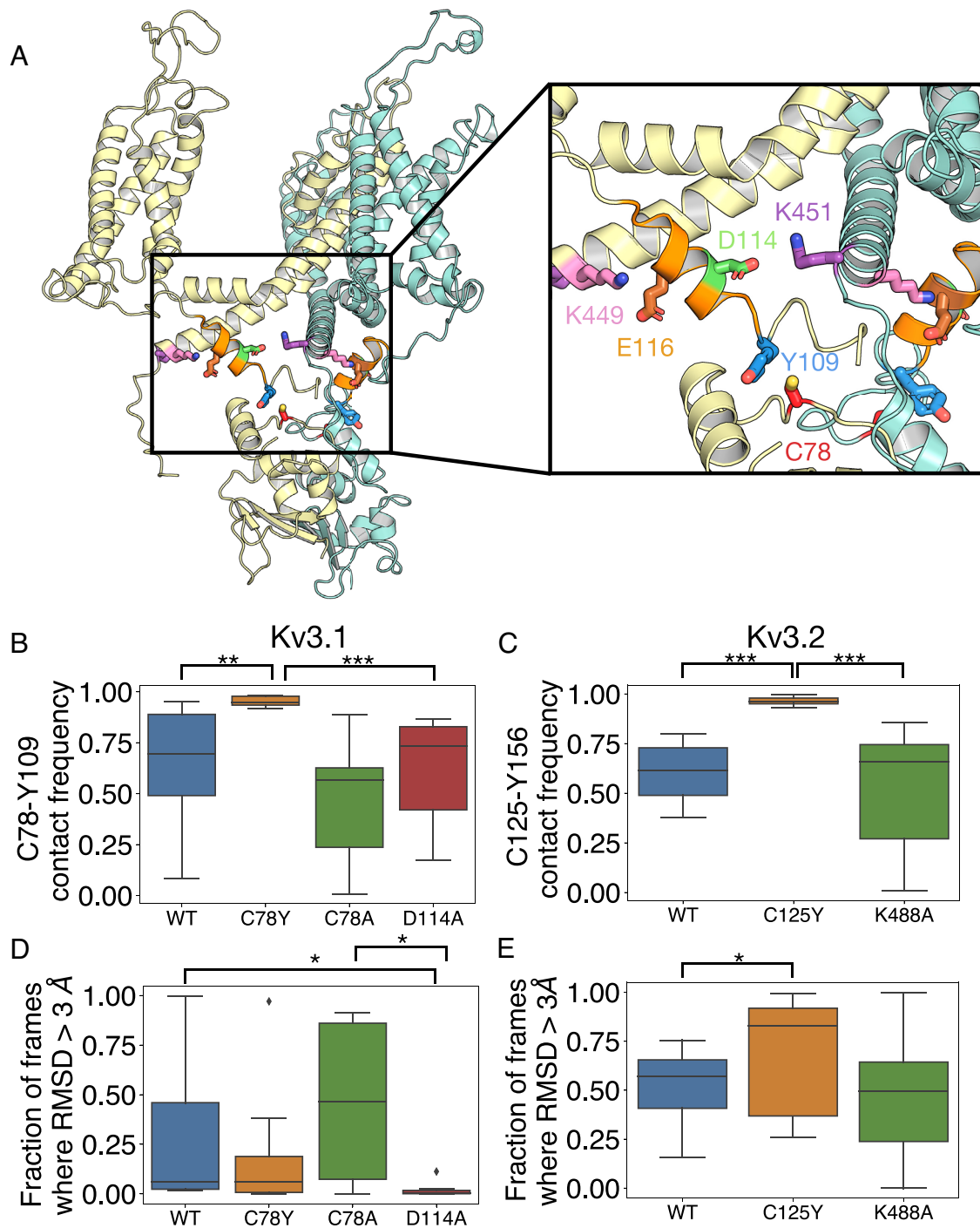
Fig. 4. Interactions around Kv3.1-Cys78, the paralogue to Kv3.2-Cys125. (*A*) Shown is a cartoon representation of the structure of K3.1, with only two adjacent subunits (*yellow* and *teal*) included for clarity. Key interacting residues Cys78 (C78, *red*), Tyr109 (Y109, *blue*), Asp114 (D114, *green*), Glu116 (E116, *brown*), Lys449 (K449, *pink*), and Lys451 (K451, *purple*) are shown as sticks. The alpha-6 helical region (residues 110 to 20) is shown in *orange*. (*B–E*) Box plot representation of distributions where the box represents the interquartile range (IQR) and the whisker shows the range of data within 1.5× of the IQR. Data beyond 1.5× of the IQR are shown as the diamond. All data were collected on the last 500 ns of the simulations. (*B*) The fraction of frames where Cys78 (C78Y) is within 3 Å proximity to Tyr109 on Kv3.1. (*C*) The fraction of frames where Cys125 (C125Y) is within 3 Å proximity to Tyr156 on Kv3.2 over the last 600 ns of the simulation ($n = 8$). (*D* and *E*) The fraction of frames where the rmsd of the C-alpha atoms of the alpha-6 helix is greater than 3 Å. *$P < 0.05$; **$P < 0.01$; and ***$P < 0.001$; via the Mann–Whitney *U* test.

Kv3.1 variant) and Tyr125 with Tyr156 (in the Kv3.2 variant) may be the defining common structural change that promotes a relative stabilization of the open state by changing the conformation of the α-6 helix. Kv3.1-Asp114Ala and Kv3.2-Asp161Ala may induce a similar change given their common effects on voltage-dependent gating (*SI Appendix*, Fig. S3).

A Computational Model of a Parvalbumin Interneuron Predicts Loss of Cell Function due to the Kv3.2-Cys125Tyr Variant. Kv3 channels facilitate high-frequency firing of fast-spiking parvalbumin-positive cerebral cortex GABAergic interneurons (PV-INs), and pharmacologic blockade or genetic deletion of Kv3 channels in mice leads to impaired excitability of PV-INs

(6, 7, 9); hence, Kv3 channels in PV-INs can be considered "excitatory." While the results presented thus far indicate a GoF at the level of the ion channel, we hypothesized such an effect would also lead to a loss of function (LoF) and impaired excitability of Kv3-expressing PV-INs, which in turn might underlie failure of inhibitory restraint within cerebral cortex networks and seizures/epilepsy. Using a single-compartment model (Fig. 5A), the Kv3.2 channel was adapted to have kinetics similar to those observed experimentally here, for Kv3.2-WT (mWT), Kv3.2-Cys125Tyr (mCys125Tyr), and the coexpression of both (mWT+mCys125Tyr) (Fig. 5B; see also Figs. 1 and 2). In turn, we used a morphologically realistic, multicompartment model of a PV-IN to determine the effects of altered Kv3.2 channel kinetics on neuronal output (Fig. 5C). We simulated the effect of the heterozygous nature of the mCys125Ty variant in a PV-IN by either incorporating the channel kinetics for mWT+mCys125Tyr into the PV-IN or by progressively manipulating the Kv3.2 channel toward kinetics like the mCys125Tyr variant (25 and 50% shown mCys125Tyr in Fig. 5D; see also SI Appendix, Fig. S6). We observed a dramatic additive shift and divisive modulation of the PV-IN frequency–current (F-I) output curve when incorporating Kv3.2 channels that were 25% mCys125Tyr and 75% mWT. When 50% of the Kv3.2 channels were the mCys125Tyr variant, there was a near-complete loss of neuronal output. When incorporating mWT+ mCys125Tyr channel kinetics, a mainly divisive shift was observed.

The shifts from mWT to mCys125Tyr values in opening offset (θ), closing offset (ϕ^1), and closing slope (σ^1) produced dominant changes in the F-I curves (Fig. 5E). Specifically, we performed two types of adjustment per parameter. First, we progressively adjusted a single parameter in the mWT so that it was like the mCys125Tyr variant, to explore how the pathological physiology may occur. Second, we adjusted a single parameter in the mCys125Tyr variant so that it was like the mWT, to explore primary functional targets for recovery. Changing the opening offset parameter only from mWT to mCys125Tyr values could shut down spiking altogether in the PV-IN, and changing this parameter from mCys125Tyr to mWT values could mostly recover the F-I curve of the mCys125Tyr PV-IN (with only 25% of Kv3.2 channels being Kv3.2-Cys125Tyr). The influence of other parameters on the F-I curves appears in SI Appendix, Fig. S6. The model supports the hypothesis that the Kv3.2-Cys125Tyr variant will lead to a loss of PV-IN function.

Discussion

Here, we report the functional effects of a novel variant in *KCNC2* identified in a patient with DEE and use computational modeling to generate a hypothesis as to the mechanism of dysfunction of *KCNC2*-expressing neurons that might underlie the pathophysiology of the associated disorder.

Vetri et al. first identified a de novo heterozygous variant in *KCNC2* c.1411G > C (p.Val471Leu; localized to the S6 transmembrane segment) in a child with epileptic encephalopathy and severe global developmental impairment (16). A subsequent study reported a de novo heterozygous variant in c.499G > T (p.Asp167Tyr; also in the intracellular N terminus) in a patient with NF1 with comorbid epileptic encephalopathy; the variant exhibited decreased current
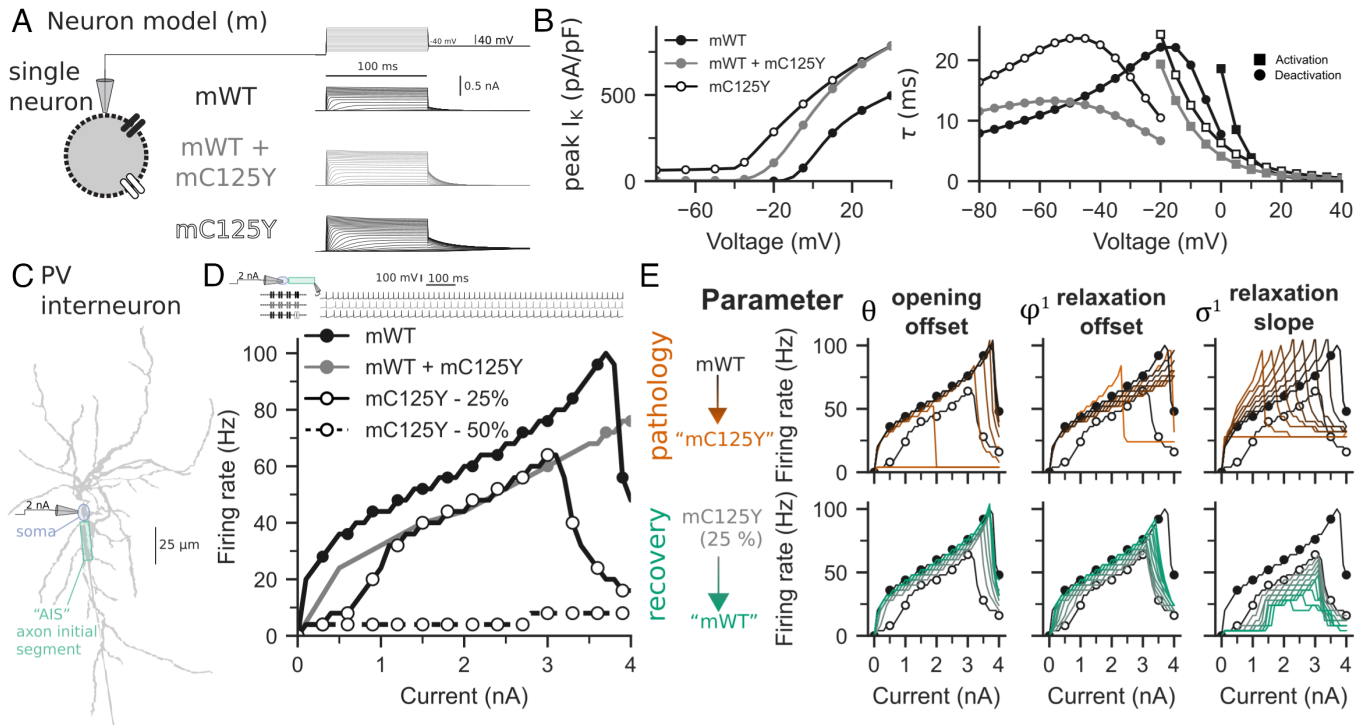

Fig. 5. A detailed PV interneuron biophysical model including WT and variant Kv3.2 reveals loss of interneuron function with expression of the Kv3.2-Cys125Tyr variant. (A) A single-compartment neuron model with either WT-like (mWT; *black*) or C125Y-like (mCys125Tyr; *gray*) Kv3.2 channels in voltage clamp (*Top*), showing corresponding K+ currents. (B) The Kv3.2 channel kinetics were fitted to experimental recordings in Figs. 2 and 3, with peak current density (*Left*), τ of activation (*circles*), and deactivation (*squares*) plotted. (C) A multicompartment morphologically realistic model of parvalbumin-positive (PV+) interneuron (PV-IN) with Kv3.2 channels. Current was injected at the soma, and the membrane potential was recorded at the axon initial segment (AIS). (D) F-I curves for mWT (*solid black*), heteromultimers of mWT and the mCys125Tyr variant (*solid gray*), and mixtures of mWT and mCys125Tyr variants (25% variant, *open circles with solid line*; 50% variant, *open circles with dashed line*). (E) The parameters controlling opening offset (*Left*), relaxation offset (*Middle*), and relaxation slope (*Right*) were primary factors in the F-I curve dysfunction for mCys125Tyr. The *Top* row shows the change in a parameter of the mWT for it to be more like the mCys125Tyr variant ("pathology," *orange*), and the *Bottom* row represents adjusting a parameter in the mCys125Tyr variant to be more like mWT ("recovery," *green*). Parameter values were evenly spaced between mWT and mCys125Tyr.

amplitude proposed to act via dominant-negative LoF effect, along with a small left-shift in the voltage-dependence of activation interpreted as GoF (18). A third report described another patient with epileptic encephalopathy and a recurrent *KCNC2*-p.Val471Leu variant (17). More recently, Schwarz et al. reported 18 patients with various forms of epilepsy found to have variants in *KCNC2*, including *KCNC2*-p.Cys125Trp (22). We now report a patient with DEE found to harbor a *KCNC2*-p.Cys125Tyr variant, which exhibits increased current density, a left-shift in the voltage dependence of activation, accelerated activation, and slowed deactivation kinetics, consistent with a GoF resulting from a relative stabilization of the open state.

Kv3.2 is selectively expressed in fast-spiking neurons throughout the brain including parvalbumin-positive GABAergic interneurons (PV-INs) of the neocortex, hippocampus, amygdala, and striatum (8). Kv3.2 is also prominently expressed in the subthalamic nucleus, medial septum and diagonal band of Broca, and at thalamocortical terminals (31). Kv3.2 expression overlaps with that of Kv3.1; however, Kv3.2 is not expressed in the cerebellum, which may explain why *KCNC2* encephalopathy is apparently not associated with ataxia, as is seen in *KCNC1*-related disorders (and *KCNC3*-related disorders). Kv3 channels—likely heteromultimers of Kv3.1 and Kv3.2 and/or Kv3.3 subunits in cerebral cortex PV-INs—possess biophysical properties unique among K$^+$ channels and that are coordinated to facilitate high-frequency firing (4, 5). Prior studies using dynamic clamp to model a Kv3 conductance showed that Kv3 channels are optimized and in fact necessary for high-frequency action potential generation (6). Dysregulation of Kv3 channel biophysics led to impaired action potential generation n PV-INs in a mouse model of Alzheimer's disease (5×FAD mice) as demonstrated using electrophysiology and use of a PV-IN single-compartment computational model (32). Hence, integrating our findings with previous results, our prediction is that—while exhibiting GoF at the ion channel level—changes observed for the Kv3.2-p.Cys125Tyr variant act via LoF at the level of neurons.

The observed left-shift in voltage dependence of activation with the Kv3.2-Cys125Tyr variant will likely lead to activation during the upstroke of the action potential and counteract inward sodium current; slowed deactivation kinetics will make it such that Kv3-mediated K$^+$ current does not completely deactivate between successive action potentials in a train, which will lead to a longer interspike interval. Hence, the observed findings are predicted to impair fast-spiking of PV-INs and lead to decreased GABAergic inhibition in cerebral cortex circuits and predispose to epilepsy and developmental impairment. The above findings are supported by the results of our computational model, which demonstrated a dominant influence of the parameters of voltage dependence of activation and deactivation for Kv3.2 on the excitability of PV-INs. In particular, shifting the voltage dependence of activation (opening offset) of Kv3.2—the most prominent abnormality observed in the voltage-clamp recordings—led to an increase in rheobase and decreased firing rate at any given current injection; incorporation of Kv3.2 channel subunits at 50% of the total Kv3 population led to near-complete cessation of neuronal firing.

The functional properties of native Kv3 channels and PV-INs in vivo will differ from the model. While multiple biophysical parameters are altered by the Kv3.2-Cys125Tyr variant, the artificial adjustment of individual parameters can provide useful indicators of functional breakdown ("pathology") and amelioration ("recovery") that highlight the discrete biophysical features that have the greatest influence on excitability. Such insights could for example suggest targets or output measures for novel pharmacotherapeutic development. Approximating heterozygosity in the

model via progressive "mixing" of channels with different kinetics is the most straightforward approach (33, 34). Approaches that simulate coexpression of variants with different kinetics may be more accurate, yet are more challenging experimentally and still not without caveats (35).

Hence, in contrast to *KCNC1*-related disorders in which the presumptive mechanism is LoF via dominant negative, our hypothesis is that the mechanism of *KCNC2* encephalopathy in this case is via GoF at the level of the ion channel, albeit with similar predicted effects on the excitability of Kv3-expressing neurons.

It is of interest to note that the mechanism of *KCNC1*-related disorders, *KCNC2* encephalopathy, and Dravet syndrome (due to pathogenic variants in *SCN1A* encoding the voltage-gated sodium channel α-subunit Nav1.1) may all converge on PV-INs based on the relative cell type–specific expression of Nav1.1 and Kv3.1/3.2 in these cells. Why patients with *KCNC2* encephalopathy do not display a Dravet syndrome-like phenotype is unclear, particularly given the similar developmental expression patterns of Nav1.1 (36, 37) and Kv3.1/3.2 (38). One possibility is that Kv3.1 and 3.2 reciprocally compensate for one another, or there is upregulation of Kv3.3 in PV-INs, whereas no other sodium channel subunit may be able to fully compensate for the heterozygous loss of Nav1.1. Alternatively, experiments in heterologous systems comparing Kv3.2-WT, Kv3.2-Cys125Tyr, and WT + Cys125Tyr combined with results of computational modeling suggest that specific biophysical features of Kv3 dysfunction—and PV-IN impairment—might underlie the cellular basis of epilepsy and neurodevelopmental impairment in this case, which is distinct from that of Dravet syndrome. Direct comparison of the GoF missense variant *KCNC2*-p.Cys125Tyr vs. LoF/heterozygous deletion of *SCN1A* on PV-INs would be of interest. However, while Kv3.2 is highly specific for PV-INs, Nav1.1 is known to be expressed in other subtypes of cerebral cortex GABAergic interneurons, which may also influence the associated phenotypes.

Structural Basis of the GoF Induced by Kv3.2-Cys125Tyr. The mechanistic underpinnings of the GoF induced by the Kv3.2-Cys125Tyr variant were not immediately clear. Kv3.2-Cys125Tyr is in the N-terminal cytoplasmic T1 domain, which is outside of the canonical voltage sensing and pore domains that control gating. By applying detailed MD simulations that leveraged the cryo-EM structure of Kv3.1, we found that both Kv3.1-Cys78Tyr and Kv3.2-Cys125Tyr may directly alter the flexibility and conformation of the α-6 helix of the T1 domain by strengthening the interaction with nearby tyrosine residues (Tyr109 and Tyr156, respectively). However, it is unlikely that α-6 helix flexibility changes are responsible for the GoF because the MD simulations produced different structural changes when comparing the impacts of Kv3.1-Cys78Tyr and Kv3.2-Cys125Tyr. Kv3.1-Cys78Tyr restricts α-6 helix flexibility by strengthening salt bridge formation between the α-6 helix and the S4 to S5 linker and weakening the formation of the salt bridges between α-6 helix and the S6 helix. In contrast, Kv3.2-Cys125Tyr may increase α-6 helix flexibility by weakening a salt bridge between α-6 helix and the S6 helix. Consistent with these discrepancies, we also found that Asp114Ala and Lys451Ala mirror the biophysical GoF induced by Cys78Tyr in Kv3.1, whereas the equivalent substitutions in Kv3.2 produced a different pattern. Kv3.2-Lys488Ala has a minimal impact on function, but Kv3.2-Asp161Ala mirrors the biophysical GoF induced by Kv3.2-Cys125Tyr. We propose that changes in the flexibility of the α-6 helix alone do not explain the GoF induced by Cys78Tyr and Cys125Tyr in Kv3.1 and Kv3.2, respectively. More likely, the structural basis of the GoF rests on differential changes

in salt bridge stability in the vicinity of the α-6 helix and, most significantly, on strong π-π stacking interaction between tyrosine residues, one of which is from the α-6 helix and the other from equivalent substitutions at positions 78 and 125 in Kv3.1 and Kv3.2, respectively. Since the wild-type tyrosine of the interacting pair is part of the α-6 helix, a stronger Tyr-Tyr interaction may promote a conformational shift in the α-6 helix, which, through interactions with S6, results in more favorable voltage-dependent gating. This conformational shift may, however, be relatively slow and not observable in our 700 ns MD simulations. Supporting the mechanistic significance of a strong π-π stacking interaction in the T1 domain, the previously reported that the Kv3.2-Cys125Trp variant also induces a dramatic hyperpolarizing shift in voltage-dependent activation (Fig. 3 *B* and *C*). We propose that a novel π-π stacking interaction in the cT1D induces a structural change in the α-6 helix of Kv3.2 and disruption of a salt bridge between Asp161 and Lys488 (Fig. 4*C* and *SI Appendix, Fig. S4*), which exerts a favorable allosteric effect on the activated conformation of the voltage sensor of the channel; as a result, the voltage dependence of activation is rendered hyperpolarized. Consequently, as the voltage dependence of activation becomes hyperpolarized, the time constant of deactivation increases (i.e., slowed deactivation), and the time constant of activation decreases (accelerating activation). Therefore, we suggest that the *KCNC2*-p.Cys125Tyr and similar variants exhibiting this GoF phenotype induce a relative stabilization of the open state.

Conclusion

KCNC2-p.Cys125Tyr represents a rare cause of epileptic encephalopathy caused by a novel structural perturbation of the α-6 helix in the T1 domain, a region that controls the relative stability of the open conformation of the channel. Furthermore, computational modeling supports the conclusion that Kv3.2 GoF can impair high-frequency firing in Kv3.2-expressing PV-INs to promote seizures. Further investigation in advanced model systems will be required to further evaluate these conclusions. Selective blockade or downregulation of variant *KCNC2* may represent a viable approach to therapy for *KCNC2*-DEE.

Materials and Methods

Electrophysiological methods follow our previously published protocols (15, 26) and are described in detail in *SI Appendix*.

Study Subjects. The patient was enrolled in a study approved by the Institutional Review Board of The Children's Hospital of Philadelphia (#15-12226). Informed consent for participation was provided by the patient's parents as the patient was a minor and with intellectual disability.

Genetic Testing and Variant Interpretation. Trio whole exome sequencing analysis was run using relevant Human Phenotype Ontology terms such that regions corresponding to epilepsy-linked genes received additional scrutiny with at least 15× coverage. Via this platform, single nucleotide variants as well as small deletions and insertions can be detected; however, it is the case that the test does not capture or analyze all regions of the exome and may miss large structural deletions/duplications or gross chromosomal rearrangements, repeat expansions, etc., and will not identify variants localized to deep intronic regions or untranslated regions.

Data Analysis. Electrophysiological data were analyzed as per published protocols (9, 19, 20). Data for standard electrophysiological parameters were obtained from at least $n = 12$ cells from $N = 4$ separate transfections for each patch-clamp experiment with HEK-293T cells and at least two batches of oocytes for TEVC. Data were analyzed using custom Matlab scripts, Clampfit 11, Sigma Plot 11 (Systat Software, Inc., San Jose, CA) and Origin 9.1 Pro (OriginLab, Northampton,

MA). Results are presented as the mean ± SEM, and statistical significance was established using the P value calculated from a one-way ANOVA, with significance established at $P < 0.05$ and the P value reported exactly.

MDs Simulations. The structure of tetrameric human Kv3.1 (residue 7 to 464) was modeled using SwissModel. The long loop between the T1 α-6 and S1 helices that was unresolved in the cryo-EM structure was built connecting residues 126 and 159, similar to our previous study (PDB entry: 7PHI) (20). The structure of human Kv3.2 (residue 7 to 500) was taken from the AlphaFold2 EBI database based on the UniProt sequence ID: Q96PR1. The disordered regions between Pro43 and Ala92 and between Asp173 and Leu198 were removed as these residues are absent in the Kv3.1 structure. The residues lining the missing gap were then connected with a peptide bond, using SwissModel to generate a continuous monomeric chain of Kv3.2, similar to the previous Kv3.1 model. The tetrameric structure was generated by aligning the Kv3.2 channel model to the Kv3.1 tetramer, allowing the tetramer to be formed. The mutant Kv3 channels (Kv3.1-Cys78Tyr, Kv3.1-Asp114Ala, Kv3.1-Cys78Ala, Kv3.2-Cys125Tyr, and Kv3.2-Lys488Ala) were then generated using PyMOL. The structure of either wild-type or mutant Kv3 was embedded into a POPC bilayer with 271 lipids and solvated in 0.15 M KCl using CHARMM-GUI (21). All simulations were simulated with a 2 fs timestep using the CHARMM36m forcefield in GROMACS 2022.1 (https://doi.org/10.5281/zenodo.6103835). The system was then energy-minimized and equilibrated using the standard CHARMM-GUI protocol, where the last step of the protocol was extended to 5 ns. The production runs were conducted for 700 ns under 303.15 K using the v-rescale thermostat (22). The pressure of all systems was maintained at 1 bar using a C-rescale barostat (23). All simulations were carried out in duplicates, where simulation frames were saved every 0.1 ns. Data were collected from each monomer of the Kv3.1 and Kv3.2 tetramer.

Computational Model. The Kv3.2 channel was modeled according to the following equations described by the Hodgkin–Huxley formalism, as in Fujita et al. (39):

$$I_{Kv3.2} = g_{Kv3.2} m^4 h \ (V - E_K),$$

where the current flowing through the channel ($I_{Kv3.2}$) is a function of the maximal conductance ($g_{Kv3.2}$), the gating variables (activation m and inactivation h), and the driving force between the membrane potential (V) and the potassium reversal potential (E_K). The gating variables obey the following dynamics, with m used as the exemplar:

$$\frac{dm}{dt} = \frac{m_\infty(V) - m}{\tau_m(V)},$$

where m_∞ is the steady-state activation function, and τ_m is the relaxation time. Kv3.2 is thus governed by the following equations and implemented in NEURON:

$$m_\infty(V) = m_{min} + \frac{1 + m_{min}}{1 + \exp\frac{\theta - V}{k}},$$

$$\tau_m(V) = \tau_{m\,min} + \frac{\tau_{m\,max} - \tau_{m\,min}}{\exp\frac{(\phi^0 - V)}{\sigma^0} + \exp\frac{(\phi^1 - V)}{\sigma^1}},$$

where θ is the "opening offset," which controls the voltage dependence of activation and is the half-maximal voltage of activation ($V_{1/2}$); k, "opening slope," which changes the gain of the activation; ϕ^0 and ϕ^1, "relaxation offset," which models the voltage dependence of relaxation; σ^0 and σ^1, "relaxation slope," which affects the gain of the relaxation, and the $\tau_{m\,min}$ and $\tau_{m\,max}$ "relaxation range" factors that determine the scale of the relaxation. Together, the parameters for the relaxation time affect both activation and deactivation.

For the single neuron model, we adapted the detailed and realistic multicompartment model of a parvalbumin-positive neocortical fast-spiking GABAergic interneuron (PV-IN) from our previous work (34). A Kv3.2 channel was inserted into a single compartment with a passive leak current. Voltage step currents were applied as described experimentally and the K⁺ current was recorded. The time constants of activation and deactivation were measured

along with the peak K$^+$ current. Kv3.2 channel kinetics were fitted from HEK cell electrophysiological recordings for Kv3.2-WT (mWT), Kv3.2-Cys125Tyr (mCys-125Tyr), and the coexpression of both (mWT + mCys125Tyr). Data on neuronal morphology and ion channel biophysical properties were from the Blue Brain Project neocortical microcircuit portal (portal.bluebrain.epfl.ch/resources/models) (24) and formulated using Hodgkin–Huxley kinetics. Briefly, values were previously fitted using BluePyOpt to model the electrophysical characteristics of continuously firing, nonaccommodating fast-spiking PV-INs, with an extended intermittently myelinated axon (25). The model was adapted to explore the effects of altered Kv3.2 channel kinetics on PV-IN properties. Simulations were performed using NEURON and Python- (27) at 34 °C for at least 500 ms unless otherwise specified. Current was injected at the soma, and action potentials were recorded at 26.5 µm ("axon initial segment") and 1056.5 µm ("axon" or presynaptic terminal). An action potential was measured if the membrane potential crossed −20 mV. Full modeling code is available at https://github.com/ChrisCurrin/pv-kcnc2.

Data, Materials, and Software Availability. Full modeling code is available at https://github.com/ChrisCurrin/pv-kcnc2 (40).

Author affiliations: [a]Division of Neurology, The Children's Hospital of Philadelphia, Philadelphia, PA 19104; [b]The Epilepsy Neurogenetics Initiative, The Children's Hospital of Philadelphia, Philadelphia, PA 19104; [c]The Institute of Science and Technology Austria, Klosterneuburg 3400, Austria; [d]Department of Neuroscience and Vickie and Jack Farber Institute for Neuroscience, Sidney Kimmel Medical College at Thomas Jefferson University, Philadelphia, PA 19107; [e]Department of Applied Physics, Science for Life Laboratory, Royal Institute of Technology, Solna SE-171 21, Sweden; [f]The Department of Neurology, The University of Pennsylvania Perelman School of Medicine, Philadelphia, PA 19104; [g]Department of Biomedical and Health Informatics, The Children's Hospital of Philadelphia, Philadelphia, PA 19104; and [h]The Department of Neuroscience, The University of Pennsylvania Perelman School of Medicine, Philadelphia, PA 19104

1. L. Y. Jan, Y. N. Jan, Voltage-gated potassium channels and the diversity of electrical signalling. *J. Physiol.* **590**, 2591–2599 (2012).
2. G. A. Gutman *et al.*, International union of pharmacology. XLI. Compendium of voltage-gated ion channels: Potassium channels. *Pharmacol. Rev.* **55**, 583–586 (2003).
3. A. S. Lindy *et al.*, Diagnostic outcomes for genetic testing of 70 genes in 8565 patients with epilepsy and neurodevelopmental disorders. *Epilepsia* **59**, 1062–1071 (2018).
4. L. K. Kaczmarek, Y. Zhang, Kv3 channels: Enablers of rapid firing, neurotransmitter release, and neuronal endurance. *Physiol. Rev.* **97**, 1431–1468 (2017).
5. B. Rudy, C. J. McBain, Kv3 channels: Voltage-gated K+ channels designed for high-frequency repetitive firing. *Trends Neurosci.* **24**, 517–526 (2001).
6. C.-C. Lien, P. Jonas, Kv3 potassium conductance is necessary and kinetically optimized for high-frequency action potential generation in hippocampal interneurons. *J. Neurosci.* **23**, 2058–2068 (2003).
7. D. Lau *et al.*, Impaired fast-spiking, suppressed cortical inhibition, and increased susceptibility to seizures in mice lacking Kv3.2 K+ channel proteins. *J. Neurosci.* **20**, 9071–9085 (2000).
8. A. Chow *et al.*, K(+) channel expression distinguishes subpopulations of parvalbumin- and somatostatin-containing neocortical interneurons. *J. Neurosci.* **19**, 9332–9345 (1999).
9. A. Erisir, D. Lau, B. Rudy, C. S. Leonard, Function of specific K(+) channels in sustained high-frequency firing of fast-spiking neocortical interneurons. *J. Neurophysiol.* **82**, 2476–2489 (1999).
10. P. Kumar *et al.*, Native-state proteomics of Parvalbumin interneurons identifies novel molecular signatures and metabolic vulnerabilities to early Alzheimer's disease pathology. bioRxiv [Preprint] (2023). https://doi.org/10.1101/2023.05.17.541038 (Accessed 22 September 2023).
11. M. Muona *et al.*, A recurrent de novo mutation in KCNC1 causes progressive myoclonus epilepsy. *Nat. Genet.* **47**, 39–46 (2015).
12. K. L. Oliver *et al.*, Myoclonus epilepsy and ataxia due to KCNC1 mutation: Analysis of 20 cases and K+ channel properties. *Ann. Neurol.* **81**, 677–689 (2017).
13. J. Park *et al.*, KCNC1-related disorders: New de novo variants expand the phenotypic spectrum. *Ann. Clin. Transl. Neurol.* **6**, 1319–1326 (2019).
14. J. M. Cameron *et al.*, Encephalopathies with KCNC1 variants: Genotype-phenotype-functional correlations. *Ann. Clin. Transl. Neurol.* **6**, 1263–1272 (2019).
15. J. Clatot, N. Ginn, G. Costain, E. M. Goldberg, A KCNC1-related neurological disorder due to gain of Kv3.1 function. *Ann. Clin. Transl. Neurol.* **10**, 111–117 (2023).
16. L. Vetri *et al.*, A de novo heterozygous mutation in KCNC2 gene implicated in severe developmental and epileptic encephalopathy. *Eur. J. Med. Genet.* **63**, 103848 (2020).
17. M. Rydzanicz *et al.*, A recurrent de novo variant supports KCNC2 involvement in the pathogenesis of developmental and epileptic encephalopathy. *Am. J. Med. Genet. A* **185**, 3384–3389 (2021).
18. A. Rademacher *et al.*, Whole-exome sequencing in NF1-related west syndrome leads to the identification of KCNC2 as a novel candidate gene for epilepsy. *Neuropediatrics* **51**, 368–372 (2020).
19. S. Mukherjee *et al.*, Personalized structural biology reveals the molecular mechanisms underlying heterogeneous epileptic phenotypes caused by de novo KCNC2 variants. *HGG Adv.* **3**, 100131 (2022).
20. S. Wang *et al.*, Emerging evidence of genotype-phenotype associations of developmental and epileptic encephalopathy due to KCNC2 mutation: Identification of novel R405G. *Front. Mol. Neurosci.* **15**, 950255 (2022).
21. L. Li *et al.*, Investigation of novel de novo KCNC2 variants causing severe developmental and early-onset epileptic encephalopathy. *Seizure* **101**, 218–224 (2022).
22. N. Schwarz *et al.*, Spectrum of phenotypic, genetic, and functional characteristics in patients with epilepsy with KCNC2 pathogenic variants. *Neurology* **98**, e2046–e2059 (2022).
23. G. Wang, M. Covarrubias, Voltage-dependent gating rearrangements in the intracellular T1–T1 interface of a K+ channel. *J. Gen. Physiol.* **127**, 391–400 (2006).
24. J. M. Gulbis, M. Zhou, S. Mann, R. MacKinnon, Structure of the cytoplasmic beta subunit-T1 assembly of voltage-dependent K+ channels. *Science* **289**, 123–127 (2000).
25. C. Gu, Y. N. Jan, L. Y. Jan, A conserved domain in axonal targeting of Kv1 (Shaker) voltage-gated potassium channels. *Science* **301**, 646–649 (2003).
26. G. Chi *et al.*, Cryo-EM structure of the human Kv3.1 channel reveals gating control by the cytoplasmic T1 domain. *Nat. Commun.* **13**, 4087 (2022).
27. Y. Kise *et al.*, Structural basis of gating modulation of Kv4 channel complexes. *Nature* **599**, 158–164 (2021).
28. M. Kircher *et al.*, A general framework for estimating the relative pathogenicity of human genetic variants. *Nat. Genet.* **46**, 310–315 (2014).
29. R. Grantham, Amino acid difference formula to help explain protein evolution. *Science* **185**, 862–864 (1974).
30. P. Hou *et al.*, Two-stage electro-mechanical coupling of a KV channel in voltage-dependent activation. *Nat. Commun.* **11**, 676 (2020).
31. M. Weiser *et al.*, Differential expression of Shaw-related K+ channels in the rat central nervous system. *J. Neurosci.* **14**, 949–972 (1994).
32. V. J. Olah *et al.*, Biophysical Kv3 channel alterations dampen excitability of cortical PV interneurons and contribute to network hyperexcitability in early Alzheimer's. *Elife* **11**, e75316 (2022).
33. G. Berecki, A. Bryson, T. Polster, S. Petrou, Biophysical characterization and modelling of SCN1A gain-of-function predicts interneuron hyperexcitability and a predisposition to network instability through homeostatic plasticity. *Neurobiol. Dis.* **179**, 106059 (2023).
34. K. Kaneko *et al.*, Developmentally regulated impairment of parvalbumin interneuron synaptic transmission in an experimental model of Dravet syndrome. *Cell Rep.* **38**, 110580 (2022).
35. N. A. Minassian, M.-C.A. Lin, D. M. Papazian, Altered Kv3.3 channel gating in early-onset spinocerebellar ataxia type 13. *J. Physiol.* **590**, 1599–1614 (2012).
36. C. S. Cheah *et al.*, Correlations in timing of sodium channel expression, epilepsy, and sudden death in Dravet syndrome. *Channels* **7**, 468–472 (2013).
37. L. Liang *et al.*, Developmental dynamics of voltage-gated sodium channel isoform expression in the human and mouse brain. *Genome Med.* **13**, 135 (2021).
38. E. M. Goldberg *et al.*, Rapid developmental maturation of neocortical FS cell intrinsic excitability. *Cereb. Cortex* **21**, 666–682 (2011).
39. T. Fujita, T. Fukai, K. Kitano, Influences of membrane properties on phase response curve and synchronization stability in a model globus pallidus neuron. *J. Comput. Neurosci.* **32**, 539–553 (2012).
40. C. B. Currin, A structurally precise mechanism links an epilepsy-associated KCNC2 potassium channel mutation to interneuron dysfunction. GitHub. https://github.com/ChrisCurrin/pv-kcnc2. Deposited 20 December 2023.